Monthly Notices
of the
ROYAL ASTRONOMICAL SOCIETY

MNRAS **498,** 77–83 (2020)
Advance Access publication 2020 August 5

doi:10.1093/mnras/staa2271

TYC 8327-1678-1: a new super lithium-rich K giant

N. Holanda [1]★ N. A. Drake [2,3] and C. B. Pereira[1]

[1]*Observatório Nacional, Rua General José Cristino 77, CEP 20921-400, São Cristóvão, Rio de Janeiro, RJ, Brazil*
[2]*Laboratory of Observational Astrophysics, St. Petersburg State University, Universitetski pr. 28, St Petersburg 198504, Russia*
[3]*Laboratório Nacional de Astrofísica/MCTIC, Rua Estados Unidos, 154, 37504-364 Itajubá, Brazil*

Accepted 2020 July 27. Received 2020 July 26; in original form 2020 June 16

ABSTRACT

In this work, we show that TYC 8327-1678-1 is a low-mass red giant star with a super lithium abundance in its atmosphere. For this, we used high-resolution spectroscopy to determine atmospheric parameters, the chemical abundances of the light elements and the isotopic ratio $^{12}C/^{13}C$ using the spectral synthesis techniques and the equivalent width measurements. Also, we used theoretical evolutionary tracks to find out the mass and the evolutionary stage of TYC 8327-1678-1. The lithium abundance was determined using the Li I resonance doublet at 6708 Å and the subordinate line at 6104 Å that yielding a mean value of $\log \epsilon(\mathrm{Li})_{\mathrm{NLTE}} = 3.48$. The projected rotational velocity ($v \sin i$) has been determined using spectral synthesis based on the isolated Fe I lines. Our results show that TYC 8327-1678-1 has a mass of $M = 1.60 \pm 0.20\,\mathrm{M}_{\odot}$, a low rotational velocity ($v \sin i = 2.35 \pm 0.24\,\mathrm{km\,s^{-1}}$) and metallicity of $[\mathrm{Fe/H}] = +0.23 \pm 0.09$. Finally, we discuss the possibility that TYC 8327-1678-1 became a lithium-rich star after a merging event involving a red giant and a helium white dwarf.

Key words: stars: abundances – stars: chemically peculiar – stars: fundamental parameters – stars: individual: TYC 8327-1678-1.

1 INTRODUCTION

Lithium-rich red giants challenge the stellar astrophysics. These peculiar stars present overabundance of the Li – a sensitive element that should has been diluted during the first ascent of the star to the red-giant-branch (RGB) phase. The convective region deepens at this phase of stellar evolution and brings the material to the star's surface from its the interior. Despite to the drastical dilution of the Li amount in the first dredge-up process, 1 per cent to 2 per cent of the GK giants present a high Li abundance[1] and yet this is a puzzle for the standard stellar evolution and mixing models (Brown et al. 1989; Kumar, Reddy & Lambert 2011; Smiljanic et al. 2018; Gao et al. 2019; among others). Notwithstanding, the report of 'super' lithium-rich giants in the literature (stars with abundance greater than meteoric lithium abundance) is significantly scarce, with a few examples known (e.g. Drake et al. 2002; Kumar et al. 2011; Monaco et al. 2014; Adamów et al. 2015; Strassmeier et al. 2015; Zhou et al. 2018; Singh, Reddy & Kumar 2019). These rare objects are generally located near the bump in the luminosity function and/or in the clump of RGB on the H–R diagram.

Among the several scenarios proposed in the literature to explain the anomalous high lithium abundance in these cool giants, some deserves to be emphasize: the enrichment by a planet or a sub-companion accretion (Alexander 1967; Siess & Livio 1999b; Aguilera-Gómez et al. 2016); merger between a red giant star and a companion helium white dwarf (Zhang et al. 2020); accretion of enriched material ejected by nova-explosions (Gratton & D'Antona 1989) or from a thermally pulsing AGB (TP-AGB) companion (Kirby et al. 2016) and internal enrichment by fresh lithium through an extra-mixing in low-mass giants (Fekel & Balachandran 1993; Boothroyd, Sackmann & Wasserburg 1995; Sackmann & Boothroyd 1999; Holanda, Drake & Pereira 2020). The stage at which this *in situ* enrichment happens is still a matter of debate in the literature – Kumar et al. (2011) argue that the RGB clump is more populated by Li-rich stars and that this enrichment may be triggered by helium flash at RGB tip. The trigger mechanism responsible for an auto-enrichment has been discussed and eventually is considered to be related with an accretion of planets or brown dwarfs and, more recently, with tidal interactions between binary stars (Siess & Livio 1999a; Casey et al. 2019). However, Jorissen et al. (2020) reported that the binary frequency among Li-rich K giants is normal when compared to that found in a sample of giants of same spectral type, which seems to refute the hypothesis that all enrichment processes derives from tidal interactions.

Sometime ago, de La Reza, Drake & da Silva (1996) proposed that K giants undergo a sudden mass-loss process and a lithium enrichment of short duration – a cycle of approximately 10^5 yr. Sometime later, Drake et al. (2002) considered a possible high incidence of Li enrichment in rapid rotators with a mass-loss and a consequent infrared excess by accretion of some material that would act by increasing the angular momentum of the giant star: these are characteristics that do not confer on all Li-rich giants, but Rebull et al. (2015) perceived that among stars with infrared excess it is easier to find Li-rich giants.

Here, we take into account the most plausible hypotheses, olds and recents, in an attempt to elucidate the super lithium abundance found in giant TYC 8327-1678-1. For this purpose, we have organized this

★ E-mail: nacizoholanda@on.br

[1]We are adopting $\log \epsilon(\mathrm{Li}) \geq 1.50$ dex for Li-rich giants. Also, for definition, $\log \epsilon(\mathrm{Li}) \equiv \log \mathrm{N(Li)/N(H)} + 12.0$.

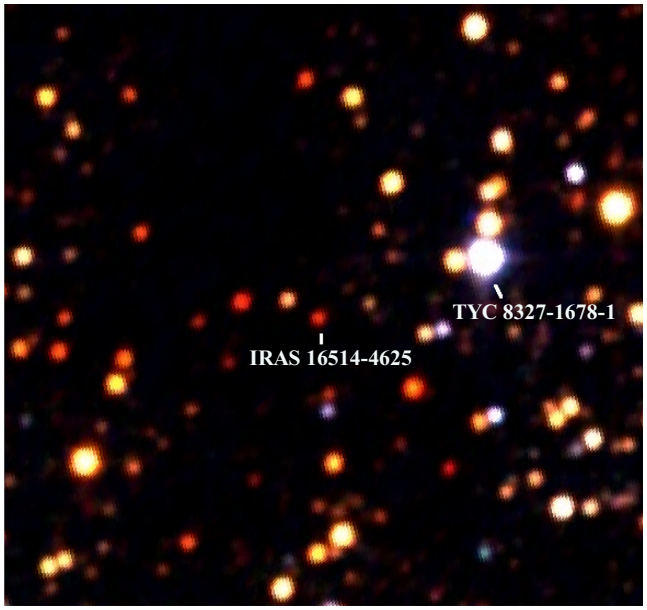

Figure 1. 2MASS image from CDS portal for IRAS 16514-4625 and TYC 8327-1678-1 (PDS 432) field. As denoted by Rebull et al. (2015), infrared source IRAS 16514-4625 has no optical equivalent.

article as follows: in Section 2, we describe our observation and give details of our analysis applied to the star TYC 8327-1678-1. In Section 3, we discuss the properties of this super lithium-rich giant in the context of the existing body of literature. Finally, concluding remarks are provided in Section 4.

2 THE GIANT TYC 8327-1678-1

TYC 8327-1678-1 was identified as lithium-rich star by de La Reza et al. (1997), who also considered this star with a possible infrared excess in the colour–colour diagram based on data from *Infrared Astronomy Satellite* (IRAS; Neugebauer et al. 1984). In a more recent study about the infrared excess associated with Li-rich K giants, Rebull et al. (2015) find this confusion in the equatorial coordinates of IRAS 16514-4625 and TYC 8327-1678-1. In other words, TYC 8327-1678-1 is not responsible for the infrared flux detected by IRAS. Fig. 1 displays the field around the two objects.

TYC 8327-1678-1 is located near the Galactic Plane ($l = 339.9$, $b = -01.9$) was previously classified as K3 III (Pickles & Depagne 2010), and has an estimated distance in $d = 844.406$ pc (Bailer-Jones et al. 2018). The main parameters estimated obtained by us in this work and those taken from the literature are given in Table 1.

2.1 Observations

The high-resolution spectrum of TYC 8327-1678-1 was obtained on 2016 March 23, with the *Fiberfed Extended Range Optical Spectrograph* (FEROS; Kaufer et al. 1999) at the 2.2 m telescope at the European Southern Observatory in La Silla, Chile. Its spectrum covers a wavelength interval between 3800 and 9000 Å and provide a resolution of $R \approx 48000$. After a data reduction process, using the FEROS pipeline, we estimated a typical signal-to-noise ratio of our spectrum of S/N ≈ 120–150.

In addition, we used photometric and astrometric information given by Henden et al. (2015) and Gaia Collaboration et al. (2018) in order to better constrain the nature of TYC 8327-1678-1.

Table 1. Derived stellar parameters of TYC 8327-1678-1.

Parameter	Value	Reference
V	11.443	Henden et al. (2015)
B−V	1.427	Henden et al. (2015)
RA (J2000)	16 55 06.193	–
Dec. (J2000)	−46 29 55.377	–
Spectral type	K3III	Pickles & Depagne (2010)
$T_{\rm eff}$ (K)	4460 ± 70	This work
log g (dex)	2.55 ± 0.10	This work
ξ (km s^{-1})	1.69 ± 0.09	This work
[Fe I/H] (dex)	+0.23 ± 0.09	This work
[Fe II/H] (dex)	+0.23 ± 0.09	This work
v sin i (km s^{-1})	2.35 ± 0.24	This work
M ($M_\odot$)	1.60 ± 0.20	This work
V_r (km s^{-1})	− 0.88 ± 0.45	This work
V_r (km s^{-1})	− 0.13 ± 0.31	Gaia Collaboration et al. (2018)
π (mas)	1.157 ± 0.044	Gaia Collaboration et al. (2018)

Table 2. Neutral and ionized iron lines.

λ	Species	χ	log gf	EW
5775.08	Fe I	4.22	−1.300	105
5848.13	Fe I	4.61	−0.900	103
5902.47	Fe I	4.59	−1.750	45
5916.25	Fe I	2.45	−2.990	136
6027.05	Fe I	4.08	−1.300	113
6093.64	Fe I	4.61	−1.410	62
6096.66	Fe I	3.98	−1.810	84
6098.24	Fe I	4.56	−1.800	62
6120.25	Fe I	0.92	−5.950	91
6151.62	Fe I	2.18	−3.300	131
6187.99	Fe I	3.94	−1.650	103
6240.65	Fe I	2.22	−3.390	130
6574.23	Fe I	0.99	−5.000	144
6703.57	Fe I	2.76	−3.150	112
6725.36	Fe I	4.10	−2.300	62
6726.67	Fe I	4.61	−1.170	89
7421.56	Fe I	4.64	−1.800	53
7547.90	Fe I	5.10	−1.100	57
7723.21	Fe I	2.28	−3.620	125
5264.81	Fe II	3.23	−3.130	48
5425.26	Fe II	3.20	−3.220	54
6247.56	Fe II	3.89	−2.300	49
6369.46	Fe II	2.89	−4.110	30
6432.68	Fe II	2.89	−3.570	50
6456.38	Fe II	3.90	−2.050	60

2.2 Atmospheric parameters

To obtain the model atmosphere for TYC 8327-1678-1 that best represents the physical conditions of its atmosphere, we first measure the equivalent widths of 19 Fe I and 6 Fe II lines using the IRAF[2] and the routine *splot*. The original list was taken from Hekker & Meléndez (2007), with features between 5700 and 7800 Å, and especially appropriate for the analysis of cool giants, avoiding lines blended with the CN lines (Table 2). These iron lines were used to constrain the best stellar atmosphere with the help of the code MOOG (2013 version; Sneden 1973) and Kurucz (Kurucz 1993) model atmospheres, considering local thermodynamic equilibrium (LTE).

[2]*The Image Reduction and Analysis Facility*.

Basically, the method consists as follows: effective temperature was derived by minimizing a slope between the abundance[3] and the lower level excitation potential (χ) of Fe I lines. Simultaneously to that, the microturbulent velocity (ξ) was found by minimizing a slope between Fe I abundance and reduced equivalent width (W_λ/λ) values. Finally, the surface gravity was obtained by imposing that the mean Fe I abundance be equal to that of the mean Fe II – ionization equilibrium. This procedure is performed by changing the value of log g until equality is reached.

The uncertainties in the atmospheric parameters were estimated following the same methodology by Holanda, Pereira & Drake (2019), i.e. the error in effective temperature was estimated from the uncertainty in the slope of relation Fe I *versus* excitation potential, while the error in the microturbulent velocity was obtained from the uncertainty in the slope of [Fe I/H]*versus* log EW/λ. For gravity, the error is estimated by changing the log g value until the difference in the average abundances of Fe I and Fe II equals the standard deviation of the mean [Fe I/H].

We better constrained the effective temperature using two other methods: (i) the line-depth ratio (LDR)[4] (Biazzo et al. 2007) and (ii) the photometric calibration (González Hernández & Bonifacio 2009). In these two cases, we found good agreement, for instance, $T_{\rm eff}$(LDR) = 4426 K and $T_{\rm eff}^{(B-V)} = 4586$ K. Previous works such as Bai et al. (2019), McDonald, Zijlstra & Watson (2017), and Ammons et al. (2006) obtained 4205, 4492, and 4466 K, respectively, that are in good agreement to one find by us based on spectroscopic analysis (also given in Table 1). In this context, we also compare the derived spectroscopic gravity with the evolutionary gravity log $g_\star$ that may be determined using the equation

$$\log g_\star = \log\left(\frac{M}{M_\odot}\right) + 0.4\,(V - A_V + BC_V) + 4,\log T_{\rm eff}^{\rm (B-V)} - 2\,\log r\,({\rm kpc}) - 16.5.$$

In the equation above, $V, A_V, BC_V, T_{\rm eff}^{\rm (B-V)}$, and r are, respectively, the visual magnitude, interstellar absorption in the V band (Chen et al. 1999), the bolometric correction (Alonso, Arribas & Martínez-Roger 1999), the photometric temperature in $(B - V)$ colour (González Hernández & Bonifacio 2009), and the distance (Bailer-Jones et al. 2018; Gaia Collaboration et al. 2018). To obtain the equation above, we adopted solar values for the absolute bolometric magnitude, surface gravity, and effective temperature, respectively, of $M_{\rm bol} = 4.75$, log $g = 4.44$ dex, and $T_{\rm eff} = 5777$ K. Finally, we find a log $g_\star = 2.53$, which is in good concordance with the value based on the spectroscopic analysis.

Despite the small difference between the values for the surface gravity, McDonald et al. (2017) found a value that is similar to that of obtained here based on spectroscopic analysis (log $g \approx 2.52$). Based on log $L/L_\odot = 1.72$ from GAIA data, our derived effective temperature and the evolutionary tracks by Girardi et al. (2000), we obtained a mass of 1.60 $M_\odot$ for a metallicity of $Z = 0.030$ (Table 1).

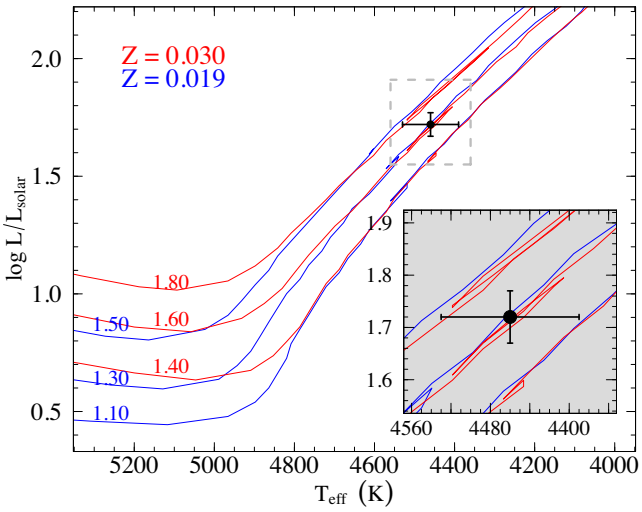

Figure 2. The location of TYC 8327-1678-1 in the $T_{\rm eff} - \log g$ diagram. The evolutionary tracks for $Z = 0.019$ (blue), while tracks for 1.8, 1.6, and 1.4 $M_\odot$ are displayed for $Z = 0.030$ (red).

Fig. 2 shows the position of TYC 8327-1678-1 in the $T_{\rm eff} - \log L$ diagram that will help us to discuss the evolutionary status of this lithium-rich star. In this graph were used tracks for $Z = 0.019$ (solar) and $Z = 0.030$, that are represented in blue and red colours, respectively.

2.3 Stellar abundances

Based on the atmospheric parameters previously determined, we obtained abundances using spectral synthesis technique for carbon, nitrogen, oxygen and lithium and also the carbon isotopic ratio ^{12}C/^{13}C, while for sodium we used equivalent width to obtain its abundance.

The lithium abundance was determined using the resonance doublet at λ 6708 and the line at λ 6104, which we assume in both cases under LTE conditions. The wavelengths and oscillator strengths for the individual components for the lithium lines were taken from Smith, Lambert & Nissen (1998) and Hobbs, Thorburn & Rebull (1999), and the *Vienna Atomic Line Database* (VALD; Kupka et al. 1999) for both lines. The resolution of the FEROS spectrum is not sufficient to rule out a contribution from ^{6}Li at λ 6708; therefore, we do not include the isotopic ratio ^{6}Li/^{7}Li in the synthesis of this feature. The fits of these two regions is shown in Fig. 3, where grey crosses represent the observed spectrum and red solid lines represent the best fit for both cases.

The carbon abundance was obtained using the C_2 (0, 1) band of Swan system $A^3\Pi_g - X^3\Pi_u$ at 5636 Å (Phillips & Davis 1968; Kovacs 1969; Lambert 1978). The nitrogen abundance and the carbon isotopic ratio ^{12}C/^{13}C were obtained by comparing the synthetic profiles of ^{12}CN and ^{13}CN lines of the 2–0 band of the CN red system $A^2\Pi - X^2\Sigma$, that are near to 8004 Å. The ^{13}CN feature is strong when the isotopic ratio ^{12}C/^{13}C is low, that is when the star is enriched in ^{13}C. The lines ^{12}C/^{13}C lines in the Swan band around 5200 Å were not used for TYC 8327-1678-1 because of they are weak since most of the carbon in this star is concentrated in form of ^{12}C. In addition, the oxygen abundance was derived from the analysis of the [O I] λ 6300.3 Å line (Allende Prieto, Lambert &

[3]For definition: [A/H] = log $(N_{\rm A}/N_{\rm H})_\star$ − log $(N_{\rm A}/N_{\rm H})_\odot$.
[4]The line ratio pairs used for LDR temperature:

V i(6199.19)/Fe i(6200.32),
V i(6213.83)/Fe i(6213.44),
V i(6224.51)/Ni i(6223.99),
V i(6243.11)/Fe i(6246.33),
V i(6251.83)/Fe i(6252.57),
V i(6256.89)/Ni i(6256.35),
V i(6268.87)/Fe i(6270.23),
Fe i(6210.67)/Fe i(6215.15),
V i(6216.36)/Fe i(6215.15),
V i(6233.20)/Fe i(6232.65),
V i(6243.11)/Fe ii(6247.56),
V i(6256.89)/Fe i(6255.95),
V i(6266.33)/Fe i(6265.14),
V i(6274.66)/Fe i(6270.23).

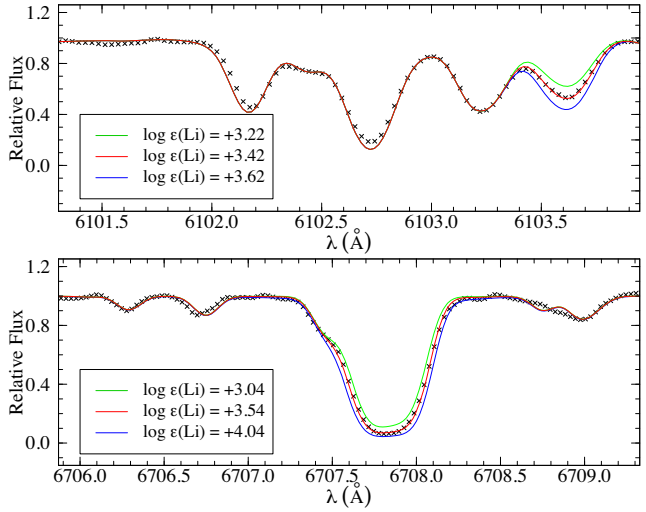

Figure 3. Best fits obtained between the synthetic and the observed FEROS spectra of TYC 8327-1678-1 around 6708 Å and 6104 Å lithium lines.

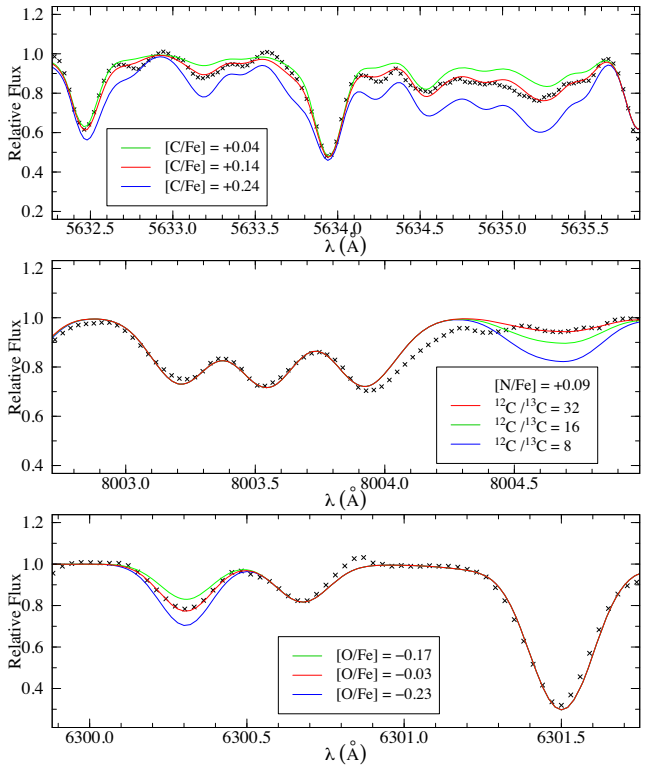

Figure 4. Best fits obtained between the synthetic (red solid lines) and the observed FEROS spectra (grey crosses) of TYC 8327-1678-1 around 5635, 8002 , and 6300 Å.

Asplund 2001). VALD was again useful in building input files for this analysis. Fig. 4 shows these three regions and with their best fits obtained using the code MOOG.

As mentioned before, the sodium abundance was obtained by measuring the equivalent widths of the doublet lines at 6154 Å and 6161 Å where log gf were taken from Reddy et al. (2003). The abundances obtained by these two lines do not significantly differ from each other (log $\epsilon(\mathrm{Na})_{\lambda 6154} = 6.52$ and log $\epsilon(\mathrm{Na})_{\lambda 6161} = 6.50$) and we adopt the average as the final abundance in LTE conditions.

Table 3. Derived chemical abundances of TYC 8327-1678-1. The last column refers to solar values adopted by Asplund et al. (2009).

Species	log ϵ(X)$_{\mathrm{LTE}}$	log ϵ(X)$_{\mathrm{NLTE}}$	[X/Fe]	log ϵ(X)$_{\odot}$
Li I $_{\lambda 6104}$	3.42	3.59	–	1.05
Li I $_{\lambda 6708}$	3.54	3.37	–	–
C (C_2)	8.80	–	+0.14	8.43
N (CN)	8.15	–	+0.09	7.83
O I	8.89	–	−0.03	8.69
$^{12}C/^{13}C$	≥32	–	–	–
Na I	6.51	6.43	−0.04	6.24

Table 4. Influence of the errors in atmospheric parameters over the abundances of elements analysed.

Species	ΔT_{eff} (+ 70)	Δ log g (+ 0.10)	ξ (+0.09)	$(\Sigma\,\sigma^2)^{1/2}$
Li I $_{\lambda 6104}$	+0.04	+0.01	−0.01	±0.04
Li I $_{\lambda 6708}$	+0.02	−0.03	−0.06	±0.07
C (C_2)	+0.01	+0.02	+0.02	±0.03
N (CN)	−0.02	+0.00	−0.03	±0.04
O I	+0.02	+0.05	+0.01	±0.05
Na I	+0.06	+0.00	−0.03	±0.07

It is well known that lithium and sodium lines in giants suffer significant non-LTE effects. In this sense, we have calculated non-local thermodynamic equilibrium (NLTE) abundances for Li and Na abundances with a grid of corrections taken from Lind, Asplund & Barklem (2009) and Lind et al. (2011), respectively. We find values of $\Delta\mathrm{Li}^{6104}_{\mathrm{NLTE}} = +0.17$ and $\Delta\mathrm{Li}^{6708}_{\mathrm{NLTE}} = -0.17$ with an average value of $\Delta\mathrm{Na}_{\mathrm{NLTE}} = -0.08$.[5] Table 3 shows all abundances for LTE and NLTE conditions that have been computed for TYC 8327-1678-1 in this work. The abundances were normalized to solar values given in Asplund et al. (2009) (log $\epsilon(\mathrm{X})_{\odot}$).

Table 4 shows the influence of the uncertainties of the atmospheric parameters over the chemical abundances for TYC 8327-1678-1. Also, the last column provide the total abundance uncertainty calculated as the root square of the sum of the various sources of uncertainties $[(\Sigma\,\sigma^2)^{1/2}]$.

3 RESULTS AND DISCUSSION

3.1 Abundances pattern

A large amount of lithium was found in the TYC 8327-1678-1's atmosphere – this quantity exceeds the meteoric abundance for this element (3.26; Asplund et al. 2009). When trying to understand how this large amount of lithium was produced and/or transferred to our target has been analysed some chemical tracers of stellar evolution and was compared our results with the other star products reported in the literature. To guide a discussion about that, we also search for ordinary low-mass giant stars (lithium-poor) and similar giant stars to our target, i.e. super lithium-rich giants, as display Fig. 5 (Brown et al. 1989; Drake et al. 2002; Reddy & Lambert 2005; Carlberg et al. 2010; Kumar et al. 2011; Monaco et al. 2014; Adamów et al. 2015; Kumar et al. 2015, 2018; Strassmeier et al. 2015; Yan et al. 2018; Zhou et al. 2018; Singh et al. 2019).

Additionally, we compared these peculiar stars with giants classified as RGB stars (with degenerate cores) or red clump stars (RC;

[5]Here, we adopted the correction value as $\Delta\mathrm{X} \equiv \log\,\epsilon(\mathrm{X})_{\mathrm{NLTE}} - \log\,\epsilon(\mathrm{X})_{\mathrm{LTE}}$.

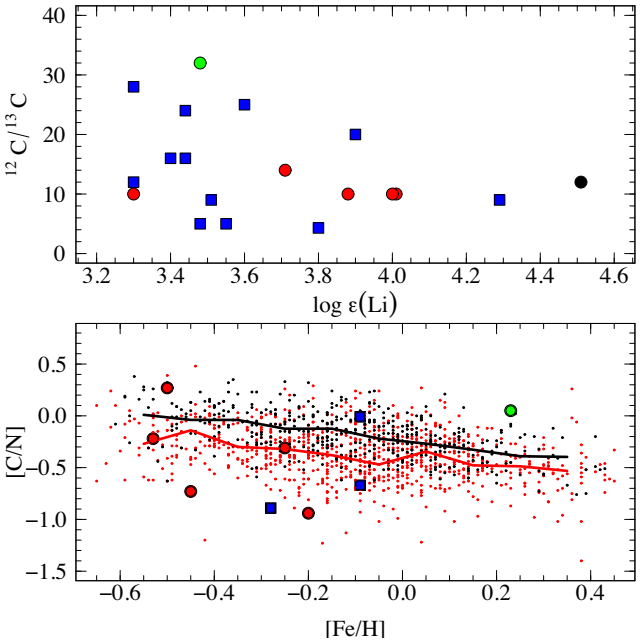

Figure 5. Distributions of log ϵ(Li) versus ^{12}C/^{13}C (top) and [C/N] versus [Fe/H] (bottom) for super Li-rich. On plots, we present normal RC (small red circles) and RGB (small black circles) stars, RC (big red circles) and RGB (big black circle) super Li-rich stars, non-classified stars (blue squares), and TYC 8327-1678-1 (green circle). Red and black solid lines constituted of a set of medians of the [C/N] at intervals of 0.10 dex in [Fe/H]. Normal stars has been chemical and asteroseismology data that were taken from Hawkins et al. (2016) and Ting et al. (2018), respectively. The super Li-rich are following: HD 9746 (Brown et al. 1989); PDS 365 (Drake et al. 2002); IRAS 13539-4153 and HD 19745 (Reddy & Lambert 2005); G0928+73.2600 (Carlberg et al. 2010); HD 8676, HD 10437, and HD 77361 (Kumar et al. 2011); Trumpler 5 3416 (Monaco et al. 2014); HD 233517 (Strassmeier et al. 2015); HD 107028 (Adamów et al. 2015); HD 19745 (Kumar et al. 2015); KIC 12645107 and KIC 2305930 (Kumar et al. 2018); TYC 3251-581-1 (Zhou et al. 2018); TYC 429-2097-1 (Yan et al. 2018); TYC 1751-1713-1 and HD 24960 (Singh et al. 2019).

burning helium in the core) based on asteroseismology data (Ting, Hawkins & Rix 2018; Hawkins et al. 2016). Looking at Fig. 5, it appears that the group of giant stars with less lithium in the atmosphere have a larger amplitude in the possible values of ^{12}C/^{13}C: despite of scarcity of objects with very high lithium, the low carbon isotopic ratio is a common feature. Furthermore, TYC-8327-1678-1 presents the higher carbon-12 abundance among these super Li-rich and Li-poor giant stars.

It is expected that a significant dilution of carbon is observed at the same time with an increase in the amount of nitrogen in the RGB of the star atmosphere. Hereupon, we identified a moderate carbon abundance [log ϵ(C) = 8.80] and a not so high nitrogen abundance [log ϵ(N) = 8.15] in TYC 8327-1678-1 atmosphere, which gives an abundance ratio of [C/N] = +0.05. In Fig. 5 (bottom), we plotted [C/N] versus [Fe/H] for normal RC (small red circles) and RGB (small black circles) stars and compare with some super Li-rich giants: there is a slight difference between the means (solid lines), but the large spread of RC stars compromises any categorization based on these abundances and it is opportune to emphasize the high [C/N] of TYC-8327-1678-1 to its iron abundance.

Unlike lithium, the sodium abundance seems to agree with standard predictions for low-mass giants; that is, there is no enrichment for this element. The sodium enrichment is expected for intermediate-mass stars ($\geq$ 2.20 $M_\odot$) according to recent mixing models (Lagarde et al. 2012).

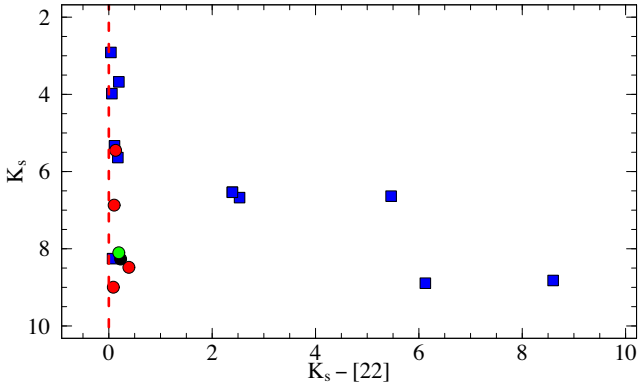

Figure 6. K_s versus K_s − [22] for a sample of super lithium-rich giants of literature and TYC 8327-1678-1. The photometric data was obtained from The Two Micron All Sky Survey (2MASS: Skrutskie et al. 2006) and Wide-field Infrared Survey Explorer (*WISE*: Wright et al. 2010). Notation is as in Fig. 5. The vertical red dashed line at K_s − [22] = 0.0 indicates no infrared excess. Here, we consider giants with infrared excess only objects with significant K_s − [22] > 0.0.

3.2 Rotational velocity and infrared excess

Rotation is a data in stellar physics that can be a very important tool in the investigation of magnetic activity, circulation of convective material and the internal structure of a giant star, and is helpful in the diagnostic of a interaction with a binary companion (Carlberg et al. 2011). In this sense, the projected rotational velocity (v sin i) of TYC 8327-1678-1 was estimated using the spectral synthesis of unblended Fe I lines – this sample is compose for lines at 5775.1, 6027.1, 6151.6, and 6302.6 Å. In this procedure, it was adopted the macroturbulent velocity that is a typical value for K giants (3.0 km s^{-1}; Fekel 1997) and a *full width at half-maximum* (FWHM) of 0.13 Å that corresponds to the FWHM of thorium-argon lines used for the wavelength calibration for FEROS spectrograph. We found a value of v sin i = 2.35 km s^{-1}, which is low but is expected for low-mass giants due to evolutionary effects, as shown by de Medeiros, Da Rocha & Mayor (1996). It is possible that the first dredge-up adds angular momentum in the convective envelope or that accretion of planets or sub-companion affects the convective envelope, but this effect is not seen in TYC 8327-1678-1.

The profile of the H α line in the spectrum of red giant stars is useful for the diagnosis of mass-loss in red giant since a possible correlation between these episodes and lithium enrichment can be true (de La Reza et al. 1996, 1997). The H α line in our giant's spectra is observed in absorption and symmetric, with equivalent width EW $\approx$ 1.03 Å and a line depth of $R_c \approx 0.25$, which are values typical for red giants according to Eaton (1995). Reinforcing this idea, the Na D lines at λ5890 do not show any additional minor lines shift in relation to the central lines.

Fig. 6 shows a colour–magnitude diagram that is useful to identify giants with some infrared excess. In this plot, we make a point for TYC 8327-1678-1 that do not have a significant infrared excess as was reported to IRAS 16514-4625 by de La Reza et al. (1997). Furthermore, only five super lithium-rich giants in this sample present larger infrared excesses. Larger infrared excesses are relatively rare in the literature, but according to Rebull et al. (2015) are at least twice as common among Li-rich K giants.

3.3 Scenarios of lithium enrichment

Based on the results presented above in Section 3, we attach hypotheses that can elucidate a probable scenario for lithium amount found in the atmosphere of TYC 8327-1678-1. Our atmospheric parameters and luminosity derived from GAIA data showed that TYC 8327-1678-1 lies at an ambiguous region between RGB-bump and red clump, if we consider the uncertainties, as seen in Fig. 2. This region is vastly populated by Li-rich giants reported in the literature. Probably, the best answer for this question about its classifying is in asteroseismology data. However, TYC 8327-1678-1 does not have any data of asteroseismology nature. Knowing this, we resort to chemical signatures: in general RGB stars have higher values of [C/N] when compared to RC stars (Hawkins et al. 2016; Ting et al. 2018; Singh et al. 2019). Here, we performed a comparison based on asteroseismology data combined with chemical abundance studies (Fig. 5) for ordinary giants and a sample of main super Li-rich stars reported in the literature – some these peculiar stars have no estimate of their evolutionary stage. Even with precise measurements of abundances of carbon and nitrogen, TYC 8327-1678-1 is far from have a larger distance relative to the star averages confirmed as RGB and RC by asteroseismology.

The production of ^{7}Li atoms is based on ^{3}He atoms and follows the reaction $^{3}\mathrm{He}(\alpha, \gamma)^{7}\mathrm{Be}$ with the transport of beryllium atoms to cool regions, where conversion to lithium occurs by electron capture, i.e. $^{7}\mathrm{Be}(^{-}\mathrm{e}, \nu)^{7}\mathrm{Li}$ (Cameron & Fowler 1971). Without the beryllium-transport occurs the destruction of lithium atoms by p-capture, which depends on the mixing efficiency of which lithium may be destroyed before it reaches the surface. Degenerate helium core stars may experience some enrichment in luminosity bump, when the mean molecular weight discontinuity left over by the first dredge-up is erased, so allowing the raise of the extra mixing process. Nevertheless, the value for the isotopic carbon ratio leads us to consider an extra mixture as less probable, since significant amounts of ^{13}C is the best mixing tracer and this is not verified for TYC 8327-1678-1.

Also, we considered as unlikely a lithium enrichment from a planet or brown dwarf, whereas the lithium amount seen in atmosphere of TYC 8327-1678-1 is very high. In the first ascent to RGB, the star expands and its radio significantly increases, which can result in the engulfment of a planet or sub-companion. However, Aguilera-Gómez et al. (2016) argue that in this case the upper limit would be about $\log \epsilon(\mathrm{Li}) \approx 2.2$, which makes this scenario incompatible with the giant analysed here.

Recently, Casey et al. (2019) observed a big number of lithium-rich giants based on LAMOST data (Zhao et al. 2012; Luo et al. 2015). According to them, binary systems can drive lithium production in low-mass red giant stars: the companion, secondary star, can provide higher diffusion by tidal effect in the envelope of the primary star, allowing lithium production. However, the radial velocity obtained by analysing the Doppler shifts of the iron lines seems to be in agreement with the value estimated by the GAIA mission: the difference less than $1.0\,\mathrm{km\,s^{-1}}$ lead us to consider that this is a single star (today).

3.3.1 Helium white dwarf-red giant star merger

This year, Zhang et al. (2020) provided results that support the merging event involving a He-white dwarf with a red giant star as a possible origin of (super) Li-rich giants. Essentially, they suggest that the final surface Li abundances depend on the masses of the progenitor helium white dwarfs: $0.35 \leq M_{\mathrm{WD}} \leq 0.40$ for creating Li-rich giants. In these models, other masses also can create another class of chemically peculiar stars, such as early-R carbon stars.

For the model by Zhang et al., the He-white dwarf and the red giant star create a common envelope when they get in contact: the dwarf will merge in the helium core of giant if a spiral occurs before the entire envelope is ejected. As a product, a new object is formed. This new star presents a degenerate nucleus surrounded by a shell rich in hydrogen and will be heated by a series of He-flashes. Finally, the helium core burning is established and this new red clump star can present peculiar chemical abundances in its surface, with dependence on initial conditions of merger. This post-merger model is in good concordance with observations for the most of Li-rich giants with respect to effective temperature, surface gravity, surface luminosity, and surface abundance ($\log \epsilon(\mathrm{Li})$ and $^{12}\mathrm{C}/^{13}\mathrm{C}$). As an important limitation, rotation velocities were not included in the this post-merger models. For future works, according to the authors, the models can take into account the transport of angular momentum during the merger.

The results found here for TYC 8327-1678-1 are also in excellent agreement with the predictions for the merge model for a metallicity of $Z = 0.030$. This is the only model in the literature that can explain simultaneously the amounts of $\log \epsilon(\mathrm{Li})$ and $^{12}\mathrm{C}/^{13}\mathrm{C}$ as well as our results for surface gravity, effective temperature and luminosity. This giant star appears to have in the same evolutionary status to the sample of 30 well-studied giants compiled by Zhang et al., although not all are super lithium-rich stars. TYC 8327-1678-1 presents a temperature near to the lowest temperature in Zhang's sample and a high metallicity and atypical carbon-nitrogen ratio. Observational data such as those present in this work can add useful links for future works, since TYC 8327-1678-1 is not common even among the super Li-rich giants.

4 SUMMARY

Based on a high-resolution optical spectrum with a wide spectral coverage, we analysed the chemical composition of the giant star TYC 8327-1678-1, which has a high amount of ^{7}Li in its atmosphere. Below we present the most relevant results:

(i) The spectroscopic and photometric stellar parameters of TYC 8327-1678-1 indicate that this giant is a low-mass star which is located in an ambiguous region of the H–R diagram. To investigate its status, we used evolutionary tracks by Girardi et al. (2000) for super solar metallicity ($Z = 0.030$).

(ii) We used many well-known super Li-rich giants from the literature for comparison purpose and carry out a wide perspective about the most likely scenarios that would provide this lithium enrichment. As a whole, we find that TYC 8327-1678-1 shows high values for the [C/N] ratio (for its metallicity) and $^{12}\mathrm{C}/^{13}\mathrm{C}$ ratio, which help us to disregard the RGB bump stage and an intrinsic enrichment.

(iii) We argue that a merging event between a He white dwarf with a red giant star provides the more probable origin for this peculiar giant star. Therefore, TYC 8327-1678-1 is a red giant at clump stage, since models provided by Zhang et al. (2020) do not create final red giants with degenerate helium cores.

In view of all that has been exposed, we expect that models like the one that involves the merging of a low-mass white dwarf and a giant should be enriched with more observational constraints such as rotational velocity, since there has already been a greater incidence of lithium enrichment in rapid rotators and this is often explored in the literature.

ACKNOWLEDGEMENTS

This study is based on the observations made with the 2.2 m telescope at the European Southern Observatory (La Silla, Chile) under the agreement with Observatório Nacional and under agreement between Observatório Nacional and Max-Planck Institute für Astronomie. NH thanks the Fundação Carlos Chagas Filho de Amparo à Pesquisa do Estado do Rio de Janeiro (FAPERJ) for financial support, grant no. 2019002307. NAD acknowledges financial support by Russian Foundation for Basic Research (RFBR) according to the research projects 18-02-00554 and 18-52-06004. The use of the SIMBAD and VizieR is acknowledged.

DATA AVAILABILITY

The data underlying this article will be shared on reasonable request to the corresponding author.

REFERENCES

Adamów M., Niedzielski A., Villaver E., Wolszczan A., Kowalik K., Nowak G., Adamczyk M., Deka-Szymankiewicz B., 2015, A&A, 581, A94
Aguilera-Gómez C., Chanamé J., Pinsonneault M. H., Carlberg J. K., 2016, ApJ, 829, 127
Alexander J. B., 1967, Observatory, 87, 238
Allende Prieto C., Lambert D. L., Asplund M., 2001, ApJ, 556, L63
Alonso A., Arribas S., Martínez-Roger C., 1999, A&AS, 140, 261
Ammons S. M., Robinson S. E., Strader J., Laughlin G., Fischer D., Wolf A., 2006, ApJ, 638, 1004
Asplund M., Grevesse N., Sauval A. J., Scott P., 2009, ARA&A, 47, 481
Bai Y., Liu J., Bai Z., Wang S., Fan D., 2019, AJ, 158, 93
Bailer-Jones C. A. L., Rybizki J., Fouesneau M., Mantelet G., Andrae R., 2018, AJ, 156, 58
Biazzo K., Frasca A., Catalano S., Marilli E., 2007, Astron. Nachr., 328, 938
Boothroyd A. I., Sackmann I. J., Wasserburg G. J., 1995, ApJ, 442, L21
Brown J. A., Sneden C., Lambert D. L., Dutchover Edward J., 1989, ApJS, 71, 293
Cameron A. G. W., Fowler W. A., 1971, ApJ, 164, 111
Carlberg J. K., Smith V. V., Cunha K., Majewski S. R., Rood R. T., 2010, ApJ, 723, L103
Carlberg J. K., Majewski S. R., Patterson R. J., Bizyaev D., Smith V. V., Cunha K., 2011, ApJ, 732, 39
Casey A. R. et al., 2019, ApJ, 880, 125
Chen B., Figueras F., Torra J., Jordi C., Luri X., Galadí-Enríquez D., 1999, A&A, 352, 459
de La Reza R., Drake N. A., da Silva L., 1996, ApJ, 456, L115
de La Reza R., Drake N. A., da Silva L., Torres C. A. O., Martin E. L., 1997, ApJ, 482, L77
de Medeiros J. R., Da Rocha C., Mayor M., 1996, A&A, 314, 499
Drake N. A., de la Reza R., da Silva L., Lambert D. L., 2002, AJ, 123, 2703
Eaton J. A., 1995, AJ, 109, 1797
Fekel F. C., 1997, PASP, 109, 514
Fekel F. C., Balachandran S., 1993, ApJ, 403, 708
Gaia Collaboration et al., 2018, A&A, 616, A1
Gao Q., Shi J.-R., Yan H.-L., Yan T.-S., Xiang M.-S., Zhou Y.-T., Li C.-Q., Zhao G., 2019, ApJS, 245, 33
Girardi L., Bressan A., Bertelli G., Chiosi C., 2000, A&AS, 141, 371
González Hernández J. I., Bonifacio P., 2009, A&A, 497, 497
Gratton R. G., D'Antona F., 1989, A&A, 215, 66
Hawkins K., Masseron T., Jofré P., Gilmore G., Elsworth Y., Hekker S., 2016, A&A, 594, A43
Hekker S., Meléndez J., 2007, A&A, 475, 1003
Henden A. A., Levine S., Terrell D., Welch D. L., 2015, American Astronomical Society Meeting Abstracts #225, p. 336.16
Hobbs L. M., Thorburn J. A., Rebull L. M., 1999, ApJ, 523, 797
Holanda N., Pereira C. B., Drake N. A., 2019, MNRAS, 482, 5275
Holanda N., Drake N. A., Pereira C. B., 2020, AJ, 159, 9
Jorissen A., Van Winckel H., Siess L., Escorza A., Pourbaix D., Van Eck S., 2020, A&A, 639, A7
Kaufer A., Stahl O., Tubbesing S., Nørregaard P., Avila G., Francois P., Pasquini L., Pizzella A., 1999, Messenger, 95, 8
Kirby E. N., Guhathakurta P., Zhang A. J., Hong J., Guo M., Guo R., Cohen J. G., Cunha K., 2016, ApJ, 819, 135
Kovács I., 1969, Rotational Structure in the Spectra of Diatomic Molecules, Akademiai Kiado, Budapest
Kumar Y. B., Reddy B. E., Lambert D. L., 2011, ApJ, 730, L12
Kumar Y. B., Reddy B. E., Muthumariappan C., Zhao G., 2015, A&A, 577, A10
Kumar Y. B., Singh R., Eswar Reddy B., Zhao G., 2018, ApJ, 858, L22
Kupka F., Piskunov N., Ryabchikova T. A., Stempels H. C., Weiss W. W., 1999, A&AS, 138, 119
Kurucz R., 1993, ATLAS9 Stellar Atmosphere Programs and 2 km/s Grid. Kurucz CD-ROM No. 13. Cambridge, p. 13
Lagarde N., Decressin T., Charbonnel C., Eggenberger P., Ekström S., Palacios A., 2012, A&A, 543, A108
Lambert D. L., 1978, MNRAS, 182, 249
Lind K., Asplund M., Barklem P. S., 2009, A&A, 503, 541
Lind K., Asplund M., Barklem P. S., Belyaev A. K., 2011, A&A, 528, A103
Luo A. L. et al., 2015, Res. Astron. Astrophys., 15, 1095
McDonald I., Zijlstra A. A., Watson R. A., 2017, MNRAS, 471, 770
Monaco L. et al., 2014, A&A, 564, L6
Neugebauer G. et al., 1984, ApJ, 278, L1
Phillips J. G., Davis S. P., 1968, The Swan System of the C2 Molecule. The Spectrum of the HgH Molecule, Vol. 2, Univ. of California Press, California
Pickles A., Depagne É., 2010, PASP, 122, 1437
Rebull L. M. et al., 2015, AJ, 150, 123
Reddy B. E., Lambert D. L., 2005, AJ, 129, 2831
Reddy B. E., Tomkin J., Lambert D. L., Allende Prieto C., 2003, MNRAS, 340, 304
Sackmann I. J., Boothroyd A. I., 1999, ApJ, 510, 217
Siess L., Livio M., 1999a, MNRAS, 304, 925
Siess L., Livio M., 1999b, MNRAS, 308, 1133
Singh R., Reddy B. E., Kumar Y. B., 2019, MNRAS, 482, 3822
Skrutskie M. F. et al., 2006, AJ, 131, 1163
Smiljanic R. et al., 2018, A&A, 617, A4
Smith V. V., Lambert D. L., Nissen P. E., 1998, ApJ, 506, 405
Sneden C. A., 1973, PhD thesis, The University of Texas, Austin
Strassmeier K. G., Carroll T. A., Weber M., Granzer T., 2015, A&A, 574, A31
Ting Y.-S., Hawkins K., Rix H.-W., 2018, ApJ, 858, L7
Wright E. L. et al., 2010, AJ, 140, 1868
Yan H.-L. et al., 2018, Nat. Astron., 2, 790
Zhang X., Jeffery C. S., Li Y., Bi S., 2020, ApJ, 889, 33
Zhao G., Zhao Y.-H., Chu Y.-Q., Jing Y.-P., Deng L.-C., 2012, Res. Astron. Astrophys., 12, 723
Zhou Y. T., Shi J. R., Yan H. L., Gao Q., Zhang J. B., Zhao G., Pan K., Kumar Y. B., 2018, A&A, 615, A74

This paper has been typeset from a TEX/LATEX file prepared by the author.